Gamow-Teller matrix elements from the ^{11}B(p,n)^{11}C reaction at $E_p \approx 26$ MeV

S. M. Grimes,* J. D. Anderson, J. C. Davis, R. H. Howell, and C. Wong
Lawrence Livermore National Laboratory, Livermore, California 94550

A. W. Carpenter, J. A. Carr, and F. Petrovich
Department of Physics, Florida State University, Tallahassee, Florida 32306
(Received 3 April 1984)

New data are presented for the ^{11}B(p,n)^{11}C reaction taken at 1 MeV intervals for proton bombarding energies in the $E_p = 16$–26 MeV range. In the experiment, final states in ^{11}C up to $E_x \simeq 10$ MeV were clearly identified and differential cross sections were extracted for the first four levels in ^{11}C. The $E_p = 26$ MeV data are examined in microscopic distorted-wave approximation calculations using the wave functions of Cohen and Kurath to describe the states in ^{11}B and ^{11}C and using the G matrix interaction of Bertsch *et al.* for the effective nucleon-nucleon interaction. Gamow-Teller matrix elements for transitions to excited states in ^{11}C are extracted on the basis of these calculations, thus extending the information on Gamow-Teller matrix elements in the mass 11 systems beyond the ground state matrix element known from β decay. Throughout, the results are contrasted with existing information from electromagnetic studies of ^{11}B. It is concluded that the Cohen-Kurath model places too much Gamow-Teller strength in the low lying states of the mass 11 systems and not enough strength at higher excitation energies. In addition, this model underestimates the net contribution to $M1$ matrix elements from the isoscalar spin and current and isovector current parts of the $M1$ operator.

I. INTRODUCTION

The utility of the intermediate energy (p,n) reaction as a tool for the study of Gamow-Teller (GT) strength in nuclei has been the subject of much recent attention, mainly because of the striking clarity with which the GT strength in medium to heavy mass nuclei is seen in this reaction at $E_p > 100$ MeV.[1–4] This is largely due to the energy dependence of the ratio of the isovector spin-dependent central and spin-independent central parts of the effective nucleon-nucleon interaction ($V_{\sigma\tau}/V_\tau$) which increases significantly with increasing energy for $E_p \approx 0$–100 MeV and is maximal for $E_p \approx 100$–300 MeV.[1,2,4–6] This feature of the effective interaction can be understood from meson exchange considerations.[7] GT transitions in light nuclei have been studied for some time now using the (p,n) reaction at lower energies ($E_p < 50$ MeV), and our ability to interpret these lower energy experimental data has been significantly improved by the knowledge of the nature of the isovector parts of the effective nucleon-nucleon interaction gained from the studies of the intermediate energy (p,n) reaction discussed above.

In this paper we present new data for the population of levels in ^{11}C up to $E_x \approx 10$ MeV via the ^{11}B(p,n) reaction taken in 1 MeV steps over the energy range $E_p = 16$–26 MeV. In the experiment, differential cross sections were extracted for the first four levels in ^{11}C. These levels have $J^\pi, T = \frac{3}{2}^-, \frac{1}{2}$ ($E_x = 0.000$ MeV); $\frac{1}{2}^-, \frac{1}{2}$ ($E_x = 2.000$ MeV); $\frac{5}{2}^-, \frac{1}{2}$ ($E_x = 4.319$ MeV); and $\frac{3}{2}^-, \frac{1}{2}$ ($E_x = 4.804$ MeV), all of which are connected to the $J^\pi, T = \frac{3}{2}^-, \frac{1}{2}$ ground state of ^{11}B through GT matrix elements. Additional GT strength is expected in ^{11}C for $E_x > 8$ MeV. The present data extend the information on GT strength in the mass 11 systems beyond that available from β-decay studies, which determine only the GT matrix element for the ground state transition.[8] Complementary information on the transitions to the ^{11}B analogs of the ^{11}C states of interest here is also available from electron scattering[9–11] and Coulomb excitation studies.[12]

The present work is part of a continuing study of low energy ($E_p < 50$ MeV) nucleon scattering from light nuclei being performed at the Lawrence Livermore National Laboratory. In earlier work differential cross sections, spin-flip cross sections, and deexcitation γ-ray angular distributions for the 1^+, 0 ($E_x = 12.71$ MeV) and 1^+,1 ($E_x = 15.11$ MeV) levels in ^{12}C have been studied[13,14] and the available (p,p′) and (p,n) data for the excitation of low lying states in the mass 6 and 7 systems have been surveyed.[15] Following closely this earlier work, a simultaneous theoretical study of the present ^{11}B(p,n) data and the corresponding electromagnetic and β-decay data has been carried out. In the present study, as in Refs. 13–15, the wave functions of Cohen and Kurath[16,17] are used to describe the target states, the (p,n) reaction is treated in the distorted wave approximation (DWA), and the realistic G matrix interaction of Bertsch *et al.*[18] is used for the effective nucleon-nucleon interaction. The radial shape of the latter has been fixed on the basis of meson exchange ideas. Various aspects of the transition matrix elements for the mass 11 systems are described below and estimates of the GT matrix elements for the excited states in ^{11}C are presented. Following closely the ideas put forth in Ref. 19, the information on the GT matrix elements and the electromagnetic transition rates are combined to deter-

mine the partition of the transition matrix elements for the first four levels in mass 11 into isovector spin and isovector current plus isoscalar spin and current contributions. All results are discussed on the basis of recent estimates of the effects of configuration mixing outside the model space, mesonic exchange currents, isobar currents, and relativistic corrections for unnatural parity dipole transitions.[1,20–24]

II. EXPERIMENTAL METHOD AND RESULTS

Protons were accelerated to energies between 16 and 26 MeV by the Lawrence Livermore National Laboratory cyclograaff.[25] A 15 MeV H^- beam was extracted from the 80 cm fixed energy cyclotron and swept externally to reduce the frequency from 25 to 5 MHz. This beam was then injected into the EN tandem for acceleration to the final energy. An average beam on target of about 1 μA was obtained with a burst width of about 2.5 ns (full width at half maximum).

The target was a colloidal suspension of ^{11}B powder deposited on 6 μm thick Mylar. The binder material (polystyrene) and Mylar did not produce background neutrons in the energy range of interest. The areal thickness of ^{11}B (isotope purity 98.5%) was 6.7 mg/cm^2. Ten collimated 10.8 m flight paths with NE 213 detectors were employed for simultaneous data acquisition; the laboratory angles were 3.5, 24, 39, 54, 69, 83, 99, 113, 129, and 144 degrees.[26] To prevent overlap of low energy neutrons with high energy neutrons from a later burst, neutron detector biases of 3.5 and 5.4 MeV were employed, the higher bias being used for proton bombarding energies above 17 MeV. A detailed discussion of the efficiency of the 5.1 cm diam by 5.1 cm long NE 213 scintillators is presented in Ref. 27. Pulse-shape discrimination was used to reduce the gamma-ray background.

Figure 1 shows a typical time-of-flight spectrum observed at 24° at a bombarding energy of 22 MeV. The arrows indicate the expected positions for neutron groups leading to the ground state (n_0) and higher excited levels[8] (n_1–n_{11}) in ^{11}C. There is excellent agreement between the expected and observed positions of the first four levels (n_0–n_3) in ^{11}C. All of these are expected to contain GT strength. Level n_5 is the first $\frac{7}{2}^-$, $\frac{1}{2}$ state in ^{11}C while n_4, n_6, n_7, n_{10}, and n_{11} are positive parity states. None of these have any GT strength and only n_5 appears to be strongly excited in the present experiment. Levels n_8 and n_9 are the ^{11}C analogs of the $\frac{3}{2}^-$, $\frac{1}{2}$ (E_x=8.53 MeV) and $\frac{5}{2}^-$, $\frac{1}{2}$ (E_x=8.93 MeV) levels observed in the electron scattering work of Ref. 11. The corresponding neutron groups observed in the present experiment are also expected to contain GT strength. The peak labeled γ is due to target gamma rays from a later beam burst and is greatly suppressed because of the use of pulse shape discrimination. Below channel 400 a continuum, arising from multibody breakup processes, is observed. The cutoff at about

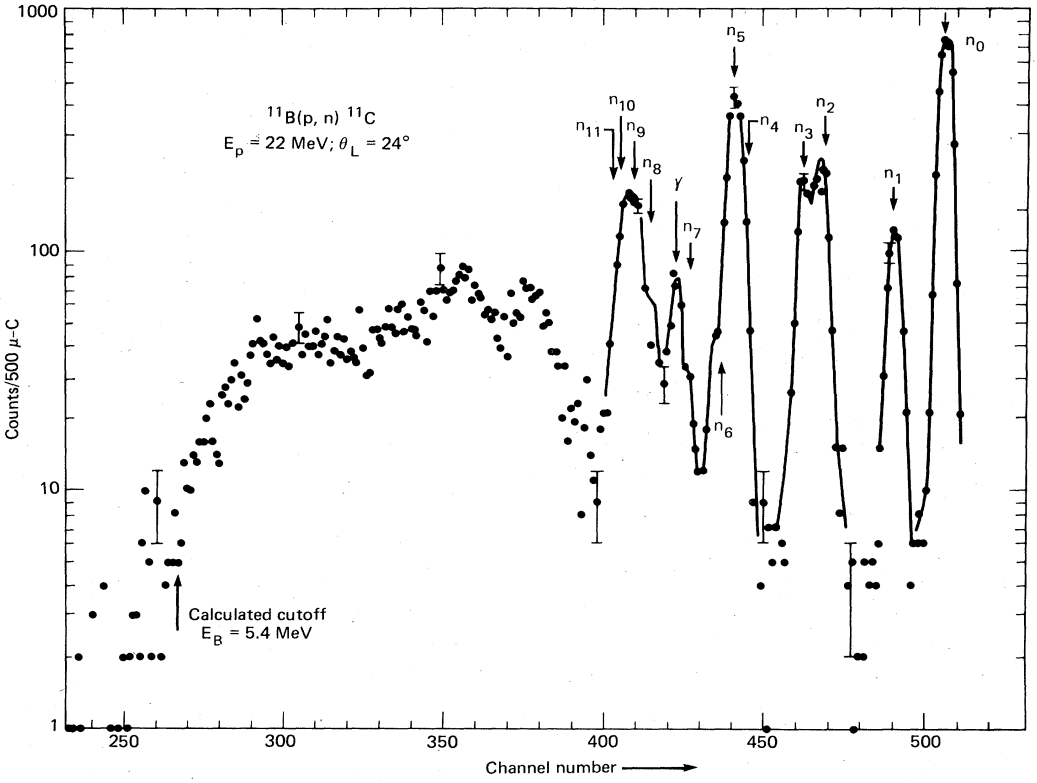

FIG. 1. Time-of-flight spectrum observed at θ_L=24° for a proton bombarding energy of 22 MeV. Time calibration of the system is 0.639 ns/channel and increasing flight time is to the left. See the text for identification of peaks in the spectrum. The solid line is a smooth curve through the measured points. The arrow at channel 266 is the calculated cutoff for a detector bias of 5.4 MeV. The neutron detector efficiency varies by only 12% over the region extending from n_0 to n_{11}.

channel 266 is due to the detector bias.

Angular distributions for the ground-state and first three excited state transitions were obtained by summing the counts in the corresponding neutron groups. Because of the low background levels underlying these neutron groups (see Fig. 1), background subtraction was not a major consideration. Above 23 MeV, n_2 and n_3 were not adequately resolved and only the summed cross sections were determined. Between 20 and 23 MeV, the counts in n_2 and n_3 were determined by a graphical decomposition of the partially resolved peaks. This is possible since the peak position and line shapes are known. Below 20 MeV n_2 and n_3 were completely resolved.

The measured angular distributions for neutron groups n_0-n_3 are displayed in Figs. 2–5 for bombarding energies between 16 and 26 MeV. The errors shown are the larger of the statistical counting errors or $\pm 7\%$, the latter error reflecting the uncertainty in the absolute detector efficiency. There is in addition a scale factor error of $\pm 15\%$ due to the nonuniformity of the colloidal target. The differential cross sections at 18 MeV are in agreement with the previously published 18 MeV data[28] taken with the 90-inch cyclotron at this laboratory. Figure 6 presents the energy dependence of the integrated cross sections over the range 16–26 MeV.

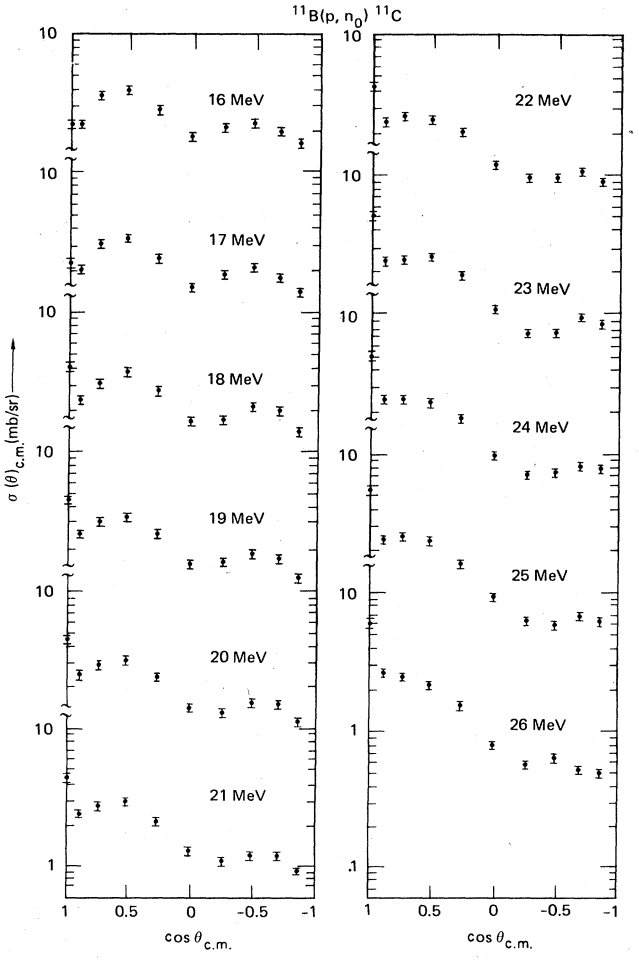

FIG. 2. Angular distributions for the ^{11}B(p,n$_0$)^{11}C reaction at energies between 16 and 26 MeV.

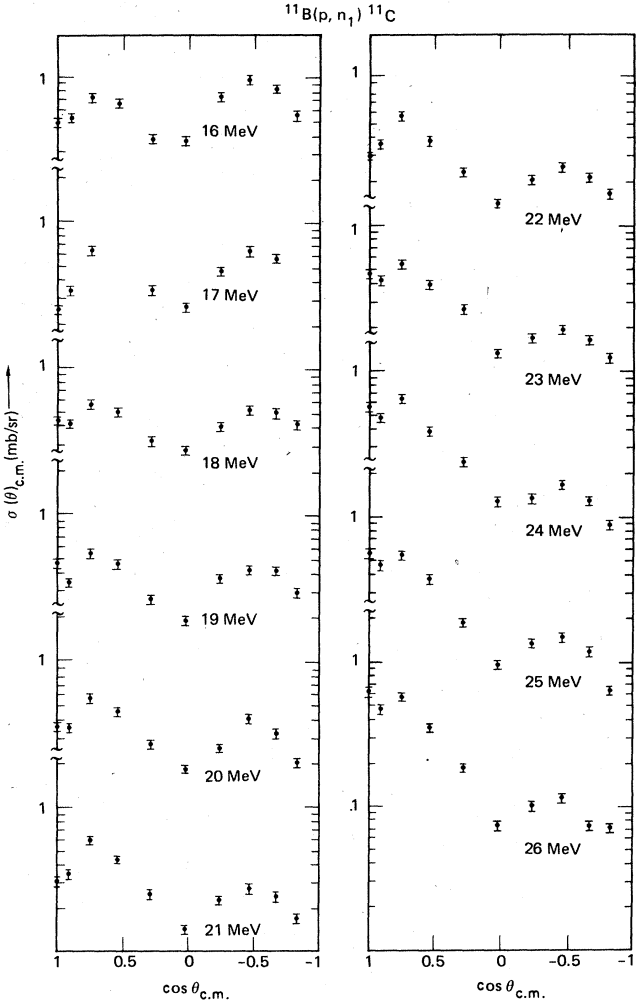

FIG. 3. Same as Fig. 2 but for the ^{11}B(p,n$_1$)^{11}C reaction.

III. THEORETICAL RESULTS

A. Electromagnetic and beta decay matrix elements

There is considerable information about levels in ^{11}B from electromagnetic studies[8–12] and the logft value for the β^+ decay of the ground state of ^{11}C to the ground state of ^{11}B is known.[8] In Tables I–III we compare the experimental and theoretical values (based on the wave functions of Refs. 16 and 17) of the ground state static moments for ^{11}B, the reduced transition probabilities for electromagnetic transitions in ^{11}B, and the GT matrix elements connecting the ground state of ^{11}B with the levels in ^{11}C. We have assumed harmonic oscillator radial wave functions throughout with the same constants for ^{11}B and ^{11}C. In addition, all theoretical matrix elements have been computed assuming bare g factors as described in Ref. 15. From the tables it is clear that the theoretical matrix ele-

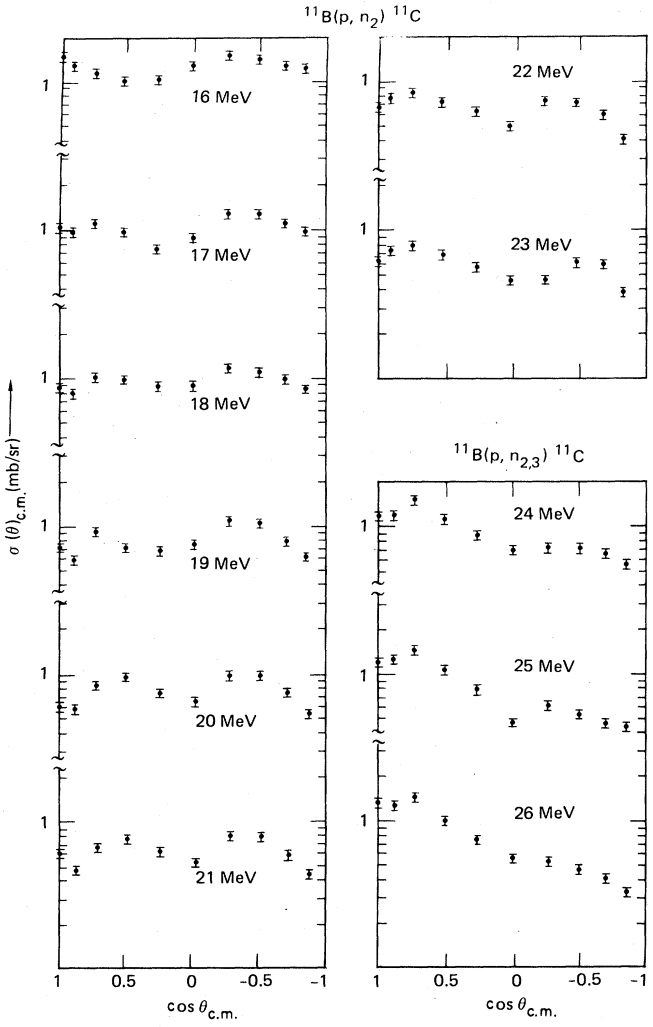

FIG. 4. Same as Fig. 2 but for the ^{11}B(p,n$_2$)^{11}C and ^{11}B(p,n$_{2,3}$)^{11}C reaction.

TABLE I. Ground state static moments for ^{11}B.

Q_{expt}[a] (e fm^2)	Q_{th}[b] (e fm^2)	μ_{expt}[a] (nm)	μ_{th} (nm)	Ω_{expt}[c] (nm fm^2)	Ω_{th}[c] (nm fm^2)
3.86	2.90	2.69	2.63	7.99	7.99

[a]Reference 8.
[b]Calculated with harmonic oscillator p-shell radial wave functions with $b=1.65$ fm deduced from fit to electric form factor for elastic electron scattering shown in Fig. 7. The experimental Q can be reproduced with $e_{eff}\approx 1.33$.
[c]Calculated with harmonic oscillator p-shell radial wave functions with $b=1.57$ fm deduced from fit to magnetic form factor for elastic electron scattering shown in Fig. 7. The experimental value for Ω is the magnitude of the value deduced from the fit of Fig. 7 which is just the value obtained from the wave functions of Refs. 16 and 17 with $b=1.57$ fm.

ments reproduce the experimental values to within roughly 30% (60% in transition rate) provided a quadrupole effective charge of about 1.5 is introduced. There are some differences between the distribution of electric quadrupole and magnetic dipole strength predicted theoretically and observed experimentally. From Table III it is also clear that the charge exchange transitions to the first four levels in ^{11}C are predicted to have substantial GT matrix elements. The total predicted GT strength for ^{11}B(p,n) is $\sum\langle GT\rangle^2=3.63$ which exceeds $3(N-Z)$ as required by the Ikeda sum rule.[1,30]

In Fig. 7 we compare the theoretical electric and magnetic elastic electron scattering form factors obtained from the wave functions of Refs. 16 and 17 with the experimental data of Refs. 9 and 10. The electric form factor contains electric monopole and quadrupole contributions and the experimental data are well described using a harmonic oscillator constant $b=1.65$ fm and a quadrupole effective charge $e_{eff}=1.38$. The latter corresponds to a quadrupole moment $Q=3.92$ e fm^2 which is in good agreement with the results of the hyperfine-structure measurement[8] given in Table I. The magnetic form factor

TABLE II. Reduced transition probabilities for electromagnetic transitions in ^{11}B.

Transition	E_x (MeV)	$B(M1\uparrow)_{expt}$[a] (e^2fm^2)	$B(M1\uparrow)_{th}$[b] (e^2fm^2)	$B(E2\uparrow)_{expt}$[c] (e^2fm^4)	$B(E2\uparrow)_{th}$[e] (e^2fm^4)	$B(M3\uparrow)_{th}$[f] (e^2fm^6)
$\frac{3}{2}^-\rightarrow\frac{1}{2}^-$	2.12	0.007±0.002	0.0112	2.1±0.4[d]	0.704	
$\frac{3}{2}^-\rightarrow\frac{5}{2}^-$	4.44	0.012±0.001	0.00881	21 ±2	8.13	0.310
$\frac{3}{2}^-\rightarrow\frac{3}{2}^-$	5.02	0.016±0.002	0.0146		0.368	1.64

[a]Reference 11. Additional $M1$ strength with an upper limit of $\sum B(M1\uparrow)=0.020\pm0.03$ e^2fm^2 is observed in the region $E_x=8$–13 MeV.
[b]Calculated from wave functions given in Ref. 17. Additional $M1$ strength with $\sum B(M1\uparrow)=0.0155$ e^2fm^2 is indicated at higher E_x in Ref. 16.
[c]Reference 11. Additional $E2$ strength with $B(E2\uparrow)=9.4\pm0.2$ and 3.6 ± 0.5 is observed at $E_x=8.57$ and 13.0 MeV, respectively.
[d]Reference 12.
[e]Calculated with harmonic oscillator p-shell radial wave functions with $b=1.65$ fm as in Table I. Experimental $B(E2\uparrow)$ can be reproduced with $e_{eff}\approx 1.61$–1.73.
[f]Calculated with harmonic oscillator p-shell radial wave functions with $b=1.57$ fm as in Table I. There is no experimental information on $B(M3\uparrow)$.

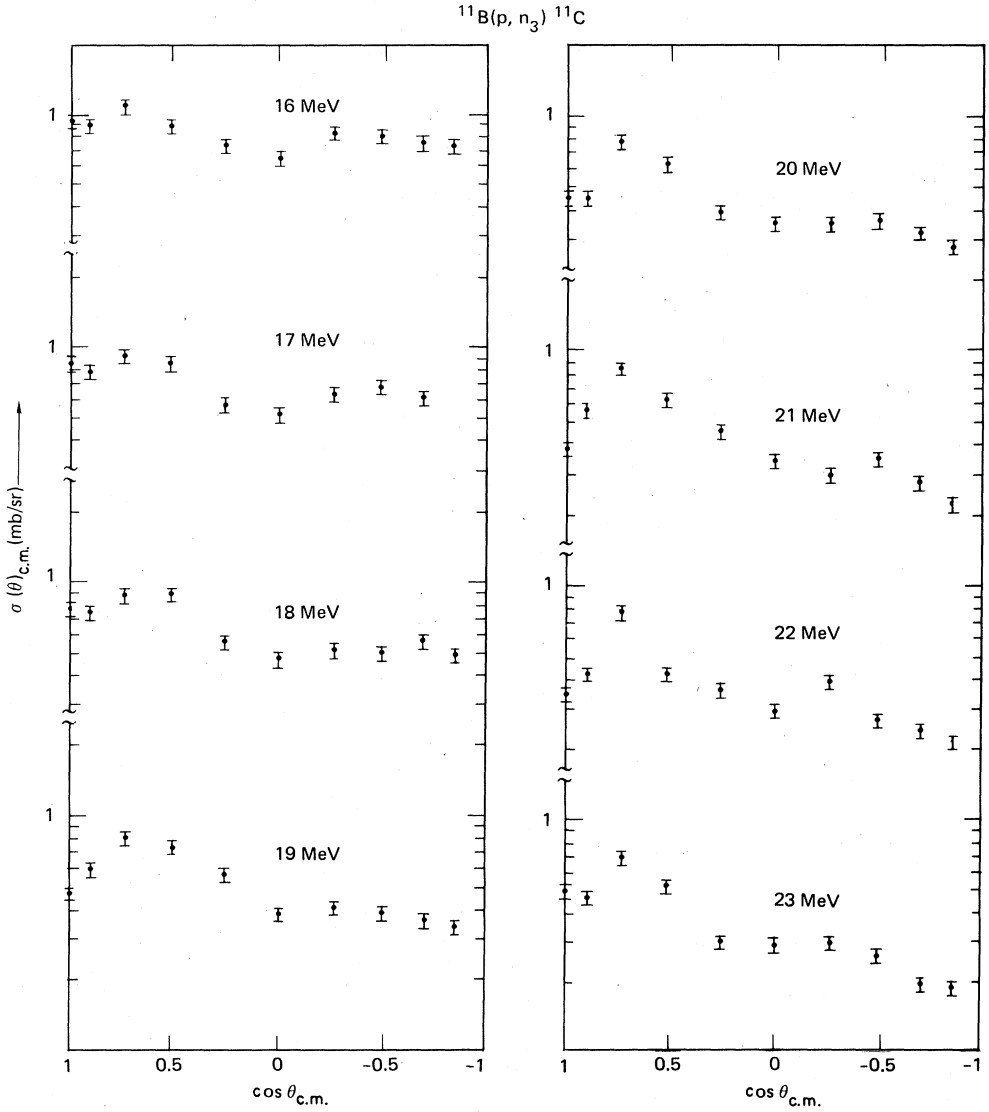

FIG. 5. Same as Fig. 2 but for the ^{11}B(p,n$_3$)^{11}C reaction.

contains magnetic dipole and octupole contributions and again the experimental data are reasonably well described by the Cohen-Kurath wave function[16,17] with $b=1.57$ fm, which is slightly smaller than obtained for the electric form factor. The magnetic octupole contribution to the magnetic form factor in Fig. 7 corresponds to a magnetic octupole moment of $\Omega=7.99$ nm fm^2 which is just the value given by the Cohen-Kurath wave functions with $b=1.57$ fm. No substantial improvement in the fit to the experimental magnetic form factor is obtained by varying the magnitude of the magnetic octupole contribution from the Cohen-Kurath value. There is a slight, but definite, deficiency in the theoretical magnetic form factor in the intermediate q range where it underestimates the experimental form factor by about 10%. One remedy for this deficiency is to increase the $L=2$ magnetic dipole transition densities by a factor of about 52. This adjustment leads to the results for the magnetic form factor shown by the dashed curve in Fig. 7. Even with this substantial increase in magnitude the net $L=2$ magnetic dipole transition density is still quite small.

Since the dipole matrix elements for the first four levels in the mass 11 systems are receiving primary attention in

TABLE III. GT matrix elements for β decay in mass 11 systems.

Transition	$\langle GT\rangle^2_{expt}$ [a]	$\langle GT\rangle^2_{th}$ [b]
$\frac{3}{2}^- \rightarrow \frac{3}{2}^-$ (g.s.)	0.386	0.625
$\frac{3}{2}^- \rightarrow \frac{1}{2}^-$		0.842
$\frac{3}{2}^- \rightarrow \frac{5}{2}^-$		0.702
$\frac{3}{2}^- \rightarrow \frac{3}{2}^-$ (e.s.)		0.792

[a]Extracted from logft value given in Ref. 8 using $\langle F\rangle^2+1.4\langle GT\rangle^2=6120/ft$ from Ref. 29. $\langle F\rangle^2$ is of course 1.
[b]Additional GT strength with $\sum\langle GT\rangle^2=0.667$ is placed at higher E_x in calculations of Ref. 16.

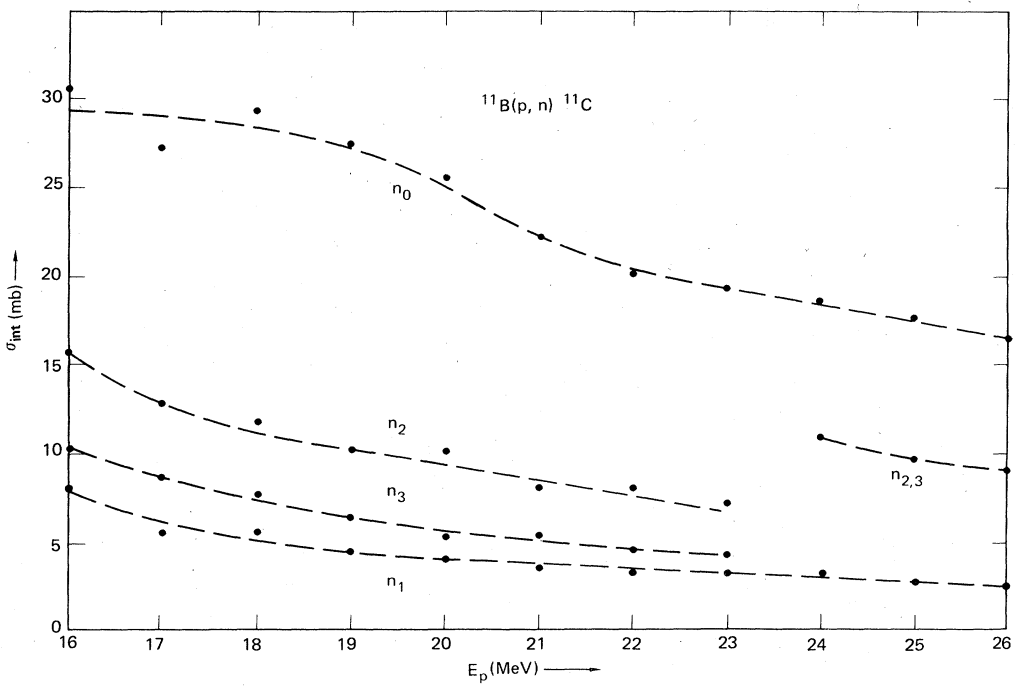

FIG. 6. Integrated cross sections for the (p,n) reaction populating the ground state and first three excited states in ^{11}C.

this work, the isoscalar and isovector spin and current $q=0$ momentum space transition densities with $J=1$, $L=0$ for these four transitions are listed in Table IV. We use the notation $\rho_{JL}^{sT}(0)$ and $\rho_{JL}^{lT}(0)$ for the spin and current densities as defined in Ref. 19. In general, all four transition densities contribute to the electromagnetic dipole matrix elements; however, the GT matrix elements for β decay and the $J=1$ contributions to the (p,n) cross sections depend, strictly and to a good approximation, respectively, only on the isovector spin densities.[1,19] From Table IV it is clear that the $J=1$ transition matrix elements are dominated by the odd proton in ^{11}B since the isoscalar and isovector transition densities tend roughly to be equal and opposite (see Ref. 15). This means that there are appreciable current and isoscalar spin contributions to the electromagnetic transition matrix elements. The current contributions are in phase with the spin contributions for the ground state matrix element and the two are out of phase for the inelastic matrix elements connecting the ground and first three excited states.

Note that the Cohen-Kurath wave functions give a value for the magnetic moment of ^{11}B that is in agreement with experiment (Table I), but overestimate the GT matrix element for the ground state β-decay transition in the mass 11 system (Table III). The latter implies that $\rho_{10}^{s1}(0)$ for the ground state in Table IV is overestimated (by about 20%). From the former we conclude that the current and isoscalar spin densities for the ground state are correspondingly underestimated or that there are substantial exchange current contributions to the magnetic moment that mask these effects. Corrections in this direction are expected from the work of Refs. 1 and 20–24. Detailed calculations for *s-d* shell nuclei[22] indicate that configuration mixing outside the model space has the net effect of reducing the magnitude of the spin densities and increasing the magnitude of the current densities. The coupling to isobar currents further reduces (increases) the coupling to the isovector spin (current) densities. For the electromagnetic matrix elements, meson exchange currents enter strongly, working against the other effects to limit the reduction (increase) in the coupling to the isovector spin (current) densities.

TABLE IV. Forward isoscalar and isovector spin and current momentum space transition densities for $J=1$, $L=0$ transition matrix elements in ^{11}B. The densities are defined in Ref. 19.

Transition	$\rho_{10}^{s0}(0)$	$\rho_{10}^{s1}(0)$	$\rho_{10}^{l0}(0)$	$\rho_{10}^{l1}(0)$
$\frac{3}{2}^- \rightarrow \frac{3}{2}^-$ (g.s.)	0.231	−0.223	0.431	−0.235
$\frac{3}{2}^- \rightarrow \frac{1}{2}^-$	−0.382	0.366	0.191	−0.232
$\frac{3}{2}^- \rightarrow \frac{5}{2}^-$	−0.156	0.193	0.078	−0.129
$\frac{3}{2}^- \rightarrow \frac{3}{2}^-$ (e.s.)	0.246	−0.251	−0.124	−0.048

B. The (p,n) reaction

Theoretical estimates of the differential cross sections for the ^{11}B(p,n)^{11}C reaction at $E_p=26$ MeV (the highest energy considered in the present experiment) have been made using the microscopic folding model and the distorted wave approximation following closely the work of Ref. 15. In particular, we have used the Reid singlet and triplet even, no triplet odd and ALTSO singlet odd central, Reid-even, Elliott-odd tensor, and Reid-odd, Elliott-even spin-orbit version of the *G*-matrix interaction of Ref. 18 as in Ref. 15. The optical parameters used in the calculations were taken from the ^{12}C study of Kolata and

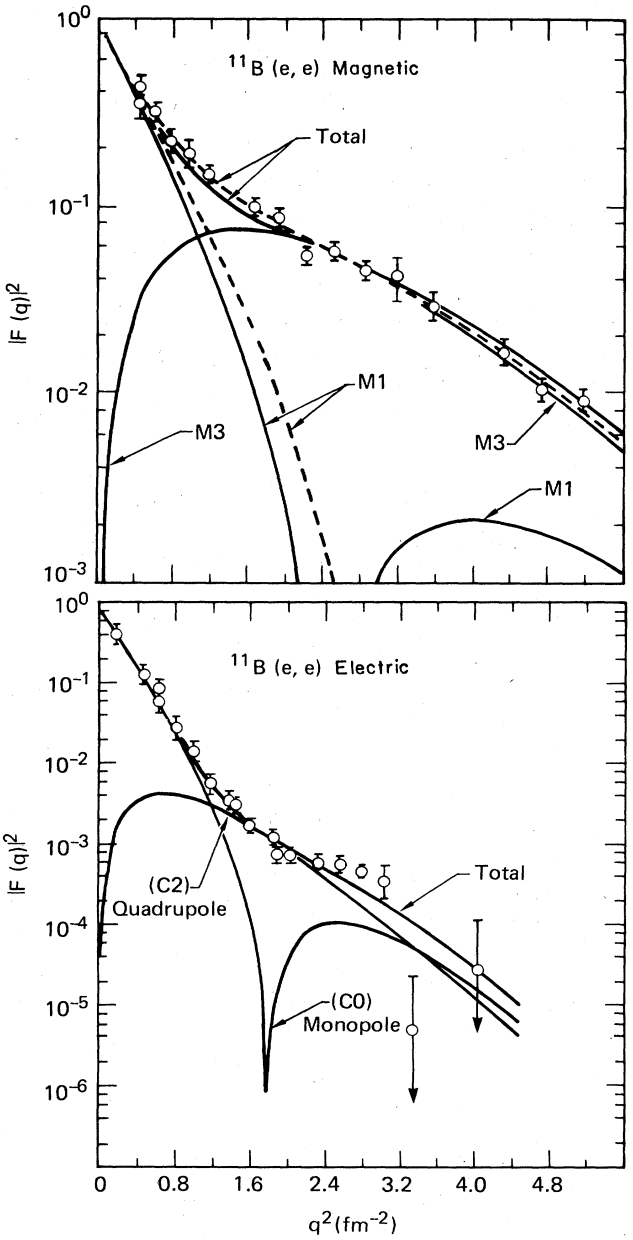

FIG. 7. The electric and magnetic form factors for elastic electron scattering from ^{11}B. The data are from Refs. 9 and 10. The solid curves are theoretical results obtained using the wave functions of Refs. 16 and 17 with the oscillator constant adjusted to give the best fit to the data. An effective charge $e_{\text{eff}}=1.38$ has been used in calculating the quadrupole contribution (C2) to the electric form factor. The dashed curves for the magnetic form factor are the results with the $L=2$ part of the magnetic dipole contribution ($M1$) increased by 51.9 as described in the text.

Galonsky.[31] The calculations were made with the computer code DWBA 70 (Ref. 32) which allows the explicit inclusion of the knockout exchange amplitudes. Finally we have used harmonic oscillator p-shell radial wave functions with $b=1.57$ fm in these calculations. This is the value determined from fitting the magnetic elastic electron scattering form factor (Fig. 7). It was selected because of our principal interest in the $J=1$ spin dipole contributions to the (p,n) cross sections. Since the above value of b was determined from electron scattering fits which include the usual harmonic oscillator center of mass correction,[33] we have also applied the corresponding approximate coordinate space center of mass correction,[34]

$$b\rightarrow\left[\frac{A-1}{A}\right]^{1/2}b=1.50\text{ fm}\,, \tag{1}$$

$$\sigma_L\rightarrow\left[\frac{A}{A-1}\right]^{L}\sigma_L\,, \tag{2}$$

to the (p,n) calculations. Here σ_L is the contribution to the total differential cross section corresponding to orbital angular momentum transfer L. For the natural parity contributions $L=J$, the total angular momentum transfer. For the unnatural parity contributions we have taken $L=J-1$, since this amplitude gives the dominant contribution to the differential cross section in these cases. This scaling of the cross sections is strictly correct only for "stretched" spatial configurations. No attempt was made to adjust the $L=2$ magnetic dipole transition densities as discussed above with reference to the dashed curve in Fig. 7.

From previous work[13–15,19] it is known that renormalization of the interaction of Ref. 18 is required to achieve consistency with experiment. For purposes of comparison with the present data we have fixed the normalization of the interaction from the $\frac{3}{2}^-\rightarrow\frac{3}{2}^-$ (g.s.) transition in the ^{11}B(p,n)^{11}C reaction since we know both the Fermi and Gamow-Teller matrix elements for this case (see Table III) which fix the corresponding isovector, $J=0$ matter and $J=1$ spin transition densities, respectively. To be specific $\sigma_{\text{pn}}(J=0)$ was taken as calculated from the Cohen-Kurath wave functions since these give the correct Fermi matrix element for the ground state to ground state transition by construction. The result for $\sigma_{\text{pn}}(J=1)$ was multiplied by

$$N_{\text{pn}}=N_\beta=\langle\text{GT}\rangle^2_{\text{expt}}/\langle\text{GT}\rangle^2_{\text{th}}=0.618$$

from Table III. This same factor was applied to $\sigma_{\text{pn}}(J=3)$, and $\sigma_{\text{pn}}(J=2)$ was reduced by a factor of 2 to roughly account for the isovector quadrupole renormalization discussed in Sec. 4.2.2 of Ref. 15. The prescription for renormalizing $\sigma_{\text{pn}}(J=1)$ and $\sigma_{\text{pn}}(J=3)$ excludes any momentum transfer and multipole dependence of the mechanism which reduces the isovector spin transition densities, for example, the presence of isobar-hole components in the nuclear wave functions.[1,21,22] The present results are not overly sensitive to these considerations, largely because of the small momentum transfers probed at the low incident proton energies in the present experiment.

With the above prescription for fixing the nuclear wave functions for the $\frac{3}{2}^-\rightarrow\frac{3}{2}^-$ (g.s.) transition in the ^{11}B(p,n)^{11}C reaction, there are still two isovector interaction strengths to be determined from a single experimental cross section, i.e., the interaction strength in the τ channel which determines $\sigma_{\text{pn}}(J=0)$ and $\sigma_{\text{pn}}(J=2)$ and that in the

$\sigma\tau$ channel which determines $\sigma_{pn}(J=1)$ and $\sigma_{pn}(J=3)$. By fixing the ratio of the two interaction normalization factors at $N_{\sigma\tau}/N_{\tau}=0.67\pm0.18$ from the $E_p\simeq25$ MeV results of Ref. 15 (mean value) and Ref. 6 (uncertainty), we deduce $N_{\tau}=0.95\pm0.10$ and $N_{\sigma\tau}=0.64\mp0.14$ from the present data which are in the mean 56% higher (25% in interaction strength) than the values obtained in Ref. 15. The 25% difference in interaction strengths for the mass 6 and 7 systems and mass 11 systems is not unreasonable given that there has been no attempt to use consistent optical parameters in the two sets of calculations. The essential results of this work depend only on the ratios of (p,n) cross sections for a given nucleus and are not affected by such considerations. We also note in passing that in the (p,n) calculations of Ref. 15 no renormalization (N_{pn}) was applied to scale the model wave functions down to the β-decay rates. In addition, contributions to the (p,n) differential cross sections corresponding to $J>1$ were not considered explicitly, but were estimated to increase the theoretical cross sections by about 10%. Since these two effects tend to be about equal and opposite, it can be assumed that the calculations of Ref. 15 are consistent with the present work even though somewhat different explicit procedures were followed. We have repeated the calculations of Ref. 15 following the procedure of the present work to confirm this directly. The complete theoretical differential cross sections for the $\frac{3}{2}^-\rightarrow\frac{3}{2}^-$ (g.s.) transition in the ^{11}B(p,n)^{11}C reaction are compared with the experimental data in Fig. 8.

The complete theoretical differential cross sections for the remaining three transitions in ^{11}B(p,n)^{11}C at $E_p=26$ MeV are shown in Fig. 9. In these calculations the interaction was renormalized in the same manner as determined above and all the $\sigma_{pn}(J=2)$ were reduced by a factor of 2 also as described above. For these three transitions $\sigma_{pn}(J=1)$ is dominant with $\sigma_{pn}(J=2)$ and $\sigma_{pn}(J=3)$ giving just 13–16 % of the total integrated cross sections.

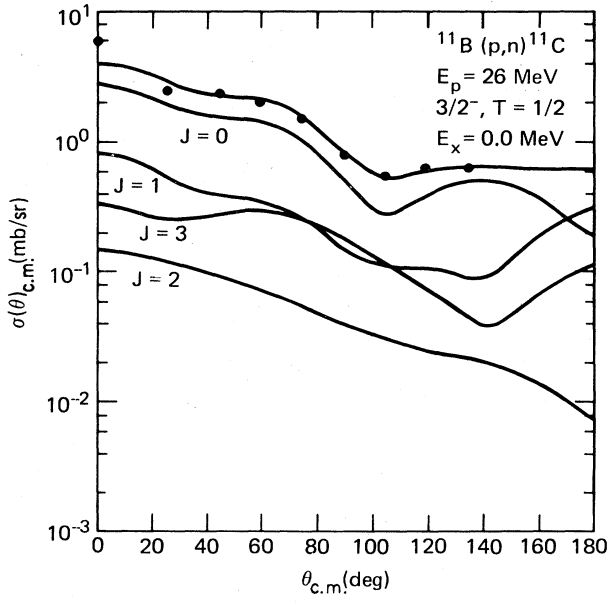

FIG. 8. Theoretical and experimental differential cross sections for the $\frac{3}{2}^-\rightarrow\frac{3}{2}^-$ (g.s.) transition in ^{11}B(p,n)^{11}C at $E_p=26$ MeV. The theoretical differential cross section is shown decomposed into contributions corresponding to $J=0$–3 total angular momentum which have been normalized as described in the text.

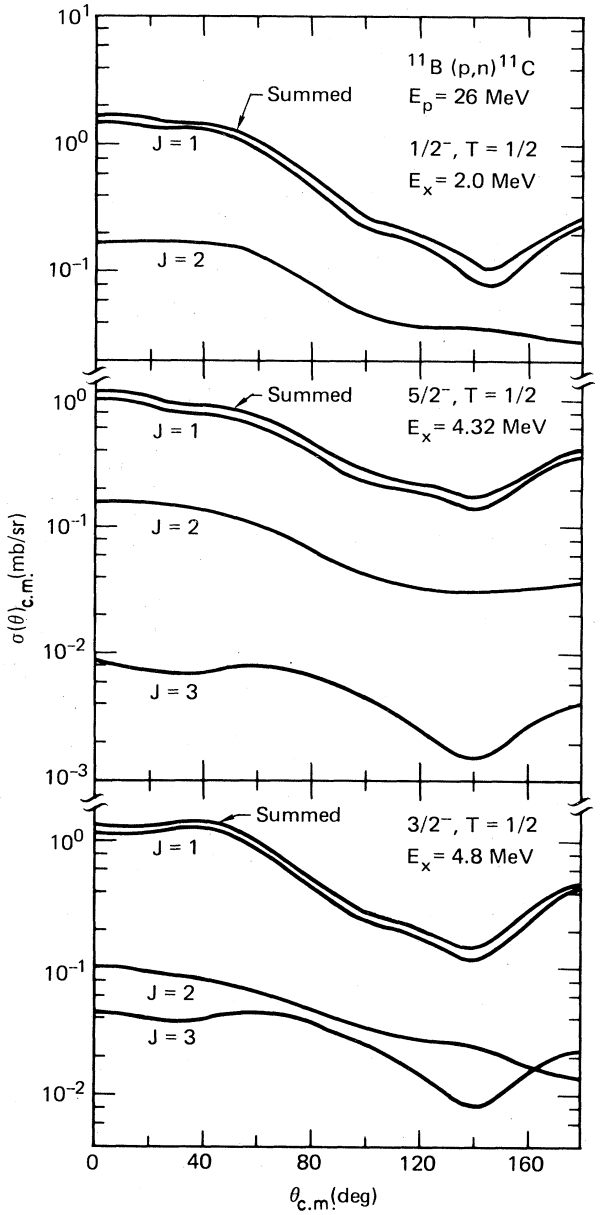

FIG. 9. Theoretical differential cross sections for the $\frac{3}{2}^-\rightarrow\frac{1}{2}^-$ ($E_x=2.000$ MeV), $\frac{3}{2}^-\rightarrow\frac{5}{2}^-$ ($E_x=4.319$ MeV), and $\frac{3}{2}^-\rightarrow\frac{3}{2}^-$ ($E_x=4.804$ MeV) transitions in ^{11}B(p,n)^{11}C at $E_p=26$ MeV obtained using the renormalized interaction deduced from the ground state transition shown in Fig. 8. The decomposition of the theoretical cross sections into contributions corresponding to separate J is shown in all cases. The $J=2$ contributions have been reduced by a factor of 2 as described in the text.

For the $\frac{3}{2}^- \rightarrow \frac{3}{2}^-$ (g.s.) transition $\sigma_{pn}(J=2)+\sigma_{pn}(J=3)$ gives 48% of the integrated cross section corresponding to $\sigma_{pn}(J=1)+\sigma_{pn}(J=2)+\sigma_{pn}(J=3)$. The complete differential cross sections for the three transitions in Fig. 9 are shown normalized to the present 26 MeV experimental data in Fig. 10. The relative contributions of the $\frac{3}{2}^- \rightarrow \frac{5}{2}^-$ and $\frac{3}{2}^- \rightarrow \frac{3}{2}^-$ (e.s.) (excited state) transitions to the unresolved $E_x \simeq 4.5$ MeV doublet were determined from the integrated cross sections for the resolved levels at $E_p=23$ MeV shown in Fig. 6. This is quite reasonable given the smooth energy dependence of the cross sections in this energy region.

The values of the normalization factors (N_{pn}) for the $\sigma_{pn}(J=1)$ differential cross sections shown in Figs. 8 and 10 are summarized in Table V and compared with the normalization factors required to reproduce the squares of the electromagnetic dipole matrix elements (Tables I and II) and $\langle GT \rangle^2$ for β decay (Table III). The latter are denoted by N_γ and N_β, respectively. Also shown in Table V are the values of $\langle GT \rangle^2$ corresponding to the (p,n) results and the ratio $N_{\beta(pn)}/N_\gamma$. The deduced values of $\langle GT \rangle^2$ suggest a different distribution of the GT strength in the first four levels than predicted by the Cohen-Kurath wave functions (Tables III and V). In particular, the second excited state is the strongest transition experimentally while the theoretical predictions suggest it should be the weakest. The experimental GT strength in these levels is, however, more reasonably correlated with the experimental distribution of $M1$ strength (see footnote c of Table V). More importantly, note that the experimental GT strength observed in the first four levels is only (58±15)% of the strength predicted by the Cohen-Kurath wave functions. The wave functions place 82% of the total theoretical GT strength in these states.

The latter results are to be contrasted with the results for the mass 6 and 7 systems where the wave functions of Cohen-Kurath place almost all of the theoretical GT strength in the first two levels and about 87% of the predicted strength is observed via β decay (Table 7 in Ref. 15). Theoretical estimates of the axial vector quenching in light nuclei[1,22] and related fits to appropriate experimental data[1,23,24] are available. These works suggest that the GT strength observed experimentally should vary from roughly 100% to 60% of the shell model value in proceeding from very light nuclei through the s-d shell nuclei. The results for the mass 6 and 7 systems quoted

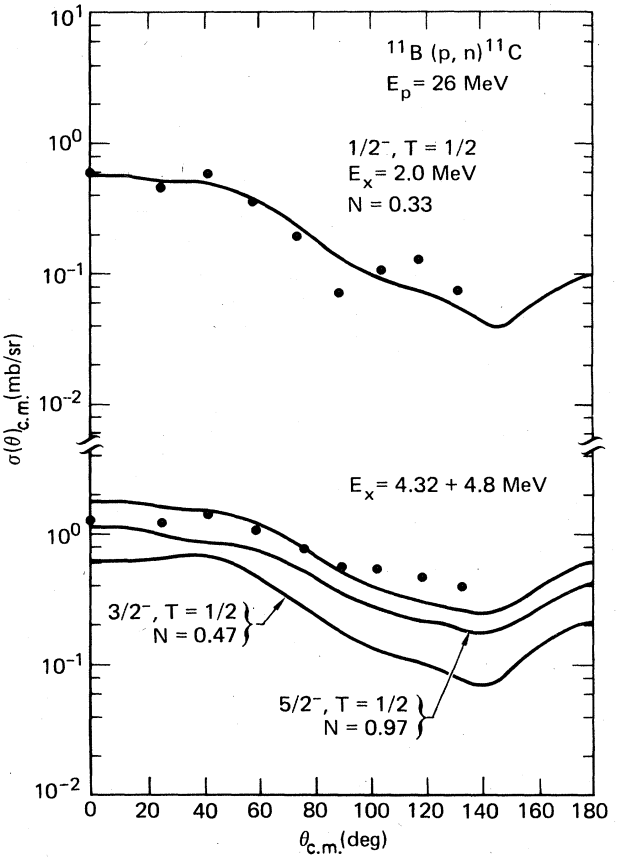

FIG. 10. Summed theoretical differential cross sections from Fig. 9 shown normalized to present $E_p=26$ MeV experimental data. The ratio of the $\frac{3}{2}^- \rightarrow \frac{5}{2}^-$ ($E_x=4.319$ MeV) and $\frac{3}{2}^- \rightarrow \frac{3}{2}^-$ ($E_x=4.804$ MeV) contributions to the unresolved $E_x=4.32$–4.80 MeV doublet was determined from the ratio of integrated cross sections at $E_p=23$ MeV where these two states were resolved. The relevant values can be obtained from Fig. 6.

TABLE V. Summary of normalization parameters for the square of dipole transition matrix elements for γ decay (N_γ), β decay (N_β), and the (p,n) reaction (N_{pn}). Also shown are the values of $\langle GT \rangle^2$ corresponding to the β decay and (p,n) results.

Transition	N_γ[a]	N_β[b]	N_{pn}[c]	$N_{\beta(pn)}/N_\gamma$[d]	$\langle GT \rangle^2$[e]
$\frac{3}{2}^- \rightarrow \frac{3}{2}^-$ (g.s.)	1.05	0.618	0.618[b]	0.589	0.386
$\frac{3}{2}^- \rightarrow \frac{1}{2}^-$	0.62±0.18		0.33±0.07	0.52±0.26	0.28±0.06
$\frac{3}{2}^- \rightarrow \frac{5}{2}^-$	1.36±0.11		0.97±0.21	0.72±0.22	0.68±0.15
$\frac{3}{2}^- \rightarrow \frac{3}{2}^-$ (e.s.)	1.10±0.14		0.47±0.10	0.43±0.15	0.37±0.08

[a]From Tables I and II.
[b]From Table III.
[c]From Fig. 10. A clearer look at the correspondence between the (p,n) reaction and the γ-decay data is obtained by comparing N_γ and $N'_{pn}=N_{pn}/\overline{N}_{pn}$, where $\overline{N}_{pn}$ is the average N_{pn}. Following the order in the table $N'_{pn}=1.04$, 0.55, 1.62, and 0.79, and $N'_{pn}/N_\gamma=0.99$, 0.89, 1.19, and 0.72.
[d]Ratios required to determine $(2\tilde{\Sigma}(0)/\tilde{g}\,{}^s_1\rho^{s\,1}_{10}(0))_{TP}$ as discussed in Sec. III C.
[e]Values deduced from (p,n) data.

above are consistent with estimates of Refs. 1 and 22–24; however, the present results for mass 11 indicate either (1) the axial vector quenching in this nucleus is fully developed to the *s-d* shell values or (2) the wave functions of Cohen-Kurath do not properly distribute the shell model strength between the first four levels and higher lying *p*-shell excitations.

In connection with these points we note that the Cohen-Kurath wave functions imply $\sum\langle \mathrm{GT}\rangle^2=0.318$ for the $\frac{3}{2}^-,\frac{1}{2}$ and $\frac{5}{2}^-,\frac{1}{2}$ levels of ^{11}C at $E_x=8.10$ and 8.42 MeV (unresolved levels n_8 and n_9 in Fig. 1). Although differential cross sections were not extracted for this group of states in the present experiment, we crudely estimate an upper limit of $\sum\langle \mathrm{GT}\rangle^2\approx 0.60$ for these levels from the spectrum in Fig. 1. Furthermore, Cohen-Kurath give $\sum B(M1\uparrow)=0.00445\ e^2\mathrm{fm}^2$ for the transitions to the analogs of these states in ^{11}B as compared to $\sum B(M1\uparrow)=0.0116\ e^2\mathrm{fm}^2$ observed in the electron scattering work of Ref. 11. Thus the Cohen-Kurath wave functions underestimate by a factor of 2 the $M1$ and GT strength in this region. The electron scattering experiment of Ref. 11 further indicates additional transverse strength at $E_x=13.0$ and 15.5 MeV in ^{11}B. This is presumably associated with $T=\frac{3}{2}$ final states. If this strength is assumed to be completely $M1$ in character, it corresponds to $\sum B(M1\uparrow)\lesssim 0.032\pm 0.007\ e^2\mathrm{fm}^2$ while Cohen-Kurath give only $\sum B(M1\uparrow)=0.0106\ e^2\mathrm{fm}^2$ for transitions to $T=\frac{3}{2}$ final states in ^{11}B. Thus we might expect to see as much as three times the $\sum\langle \mathrm{GT}\rangle^2=0.182$ predicted by Cohen-Kurath for transitions to $T=\frac{3}{2}$ final states in ^{11}C. All of this tends to support contention (2) of the preceding paragraph. It would be useful to have measurements of the ^{11}B(p,n) reaction for $E_p=100$–200 MeV to provide further information on this matter.

C. Current and isoscalar spin densities

In Ref. 19 it was demonstrated that information on electromagnetic transition rates and (p,n) cross sections (equivalently β-decay matrix elements) for $0^+,T=0\rightarrow 1^+,T=1$ transitions could be used to obtain an independent estimate of the separate isovector spin and current contributions to the transition matrix elements. For the mass 11 mirror systems being considered here, this procedure can be extended to separate the isovector spin contribution from the combined isoscalar spin and isoscalar and isovector current contributions. The argument is simply based on the fact that the ratio of the squared electromagnetic matrix elements to the (p,n) cross sections (also $\langle \mathrm{GT}\rangle^2$) is

$$R^2=C^2\left[\frac{\tilde{g}^s_1}{\tilde{g}_A}\right]^2\left[1+\frac{2\tilde{\Sigma}(0)}{\tilde{g}^s_1\rho^{s1}_{10}(0)}\right]^2, \tag{3}$$

where C is a constant incorporating reaction constants,

$$\tilde{\Sigma}(0)=\tfrac{1}{2}\tilde{g}^s_0\rho^{s0}_{10}(0)+\tilde{g}^l_0\rho^{l0}_{10}(0)+\tilde{g}^l_1\rho^{l1}_{10}(0)\ , \tag{4}$$

and $\tilde{g}^s_T$, $\tilde{g}^l_T$, and $\tilde{g}_A$ represent the electromagnetic spin and current g factors and the axial vector coupling constant. The tildes over the g factors are used to indicate effective coupling constants[1,20–24] which can be introduced to account for effects associated with nucleon structure, e.g., meson exchange currents and coupling to isobar currents, and effects due to configuration mixing outside the model space under the assumption that the densities are model space rather than "true" nuclear densities. Effective coupling constants were not considered in the work of Ref. 19. The essential idea is that if R^2/C^2 is known from the experimental data, then Eq. (3) can be used to determine the quantity $[2\tilde{\Sigma}(0)/\tilde{g}^s_1\rho^{s1}_{10}(0)]$, which provides a measure of the contribution to the transition matrix elements from the coupling to current and isoscalar spin densities relative to the coupling to the isovector spin density. From the results of the preceding two sections, in particular Tables IV and V, we have for the positive parity dipole transitions in the mass 11 systems

$$R^2=C^2\frac{N_\gamma}{N_{\mathrm{pn}}}\left[\frac{g^s_1}{g_A}\right]^2\left\{1+\left[\frac{2\Sigma(0)}{g^s_1\rho^{s1}_{10}(0)}\right]_{\mathrm{CK}}\right\}^2, \tag{5}$$

which can be combined with Eq. (3) to obtain

$$\left[\frac{2\tilde{\Sigma}(0)}{\tilde{g}^s_1\rho^{s1}_{10}(0)}\right]_{\mathrm{TP}}=\left[\frac{\tilde{g}_A/g_A}{\tilde{g}^s_1/g^s_1}\right]\left[\frac{N_\gamma}{N_{\mathrm{pn}}}\right]^{1/2}\times\left\{1+\left[\frac{2\Sigma(0)}{g^s_1\rho^{s1}_{10}(0)}\right]_{\mathrm{CK}}\right\}-1\ , \tag{6}$$

where we have introduced the notation TP for true or experimental p-shell ratio and CK for Cohen-Kurath, under the assumption that the $\tilde{g}$ contain effects associated with nucleon structure plus configuration mixing outside the p shell. The ability of the Cohen-Kurath wave function to explain the relative differences between the electromagnetic and (p,n) data (equivalently β decay) is determined by comparing $[2\Sigma(0)/g^s_1\rho^{s1}_{10}(0)]_{\mathrm{CK}}$ with $[2\tilde{\Sigma}(0)/\tilde{g}^s_1\rho^{s1}_{10}(0)]_{\mathrm{TP}}$. The true model isovector spin density $[\rho^{s1}_{10}(0)]_{\mathrm{TP}}$ may be determined from

$$\langle \mathrm{GT}\rangle^2_{\mathrm{exp}}=\left[\frac{\tilde{g}_A}{g_A}\right]^2 2\pi\frac{2J_f+1}{2J_i+1}\,|\,\alpha_T[\rho^{s1}_{10}(0)]_{\mathrm{TP}}\,|^2\ , \tag{7}$$

where the factor α_T converts the isospin transfer $M_T=0$ density $\rho^{s1}_{10}(0)$ to the $M_T=-1$ density required for the (p,n) reaction. [Equations (A21) and (A44) in Ref. 15.] $[\tilde{\Sigma}(0)]_{\mathrm{TP}}$ then follows from $[2\tilde{\Sigma}(0)/\tilde{g}^s_1\rho^{s1}_{10}(0)]_{\mathrm{TP}}$.

Table VI contains a comparison of $[2\tilde{\Sigma}(0)/g^s_1\rho^{s1}_{10}(0)]_{\mathrm{CK}}$ and $[2\tilde{\Sigma}(0)/\tilde{g}^s_1\rho^{s1}_{10}(0)]_{\mathrm{TP}}$ obtained from Eq. (6) using the N_γ and N_{pn} values from Table V and, in the spirit of contention (2) discussed at the end of the preceding section, $\tilde{g}_A/g_A=0.91$ which is appropriate for p-shell nuclei. Bare electromagnetic g factors have been assumed since these, in combination with the Cohen-Kurath wave functions, give a good average description of the electromagnetic matrix elements (Tables I and II) and $\tilde{g}^s_1/g^s_1$ is expected to be greater than $\tilde{g}_A/g_A$ on the basis of Refs. 1 and 22–24. The results in Table VI indicate that the current and isoscalar spin contributions to the $M1$ matrix elements for the first four levels in ^{11}B are underestimated by the Cohen and Kurath wave function.

TABLE VI. Comparison of the ratio $[2\tilde{\Sigma}(0)/\tilde{g}^{s}_{1}\rho^{s1}_{10}(0)]_{TP}$ obtained from Eq. (6) to the corresponding ratio obtained with model wave functions.

Transition	$[2\Sigma/g^{s}_{1}\rho^{s1}_{10}]_{CK}$[a]	$[2\tilde{\Sigma}/\tilde{g}^{s}_{1}\rho^{s1}_{10}]_{TP}$[b]
$\frac{3}{2}^{-}\rightarrow\frac{3}{2}^{-}$ (g.s.)	0.828	1.17
$\frac{3}{2}^{-}\rightarrow\frac{1}{2}^{-}$	−0.050	0.19±0.21
$\frac{3}{2}^{-}\rightarrow\frac{5}{2}^{-}$	−0.077	−0.01±0.08
$\frac{3}{2}^{-}\rightarrow\frac{3}{2}^{-}$ (e.s.)	0.119	0.56±0.15

[a]Calculated with bare g factors and densities given in Table IV derived from Cohen-Kurath wave functions.

[b]Estimate from Eq. (6) based on N_γ and N_{pn} from Table V using $(\tilde{g}_A/g_A)=0.91$ and bare electromagnetic spin and current g factors.

IV. SUMMARY

New differential cross section data have been presented for ^{11}B(p,n) to the first four levels in ^{11}C at $E_p=16$–26 MeV covering the angular range 3.5–144 degrees. The data for $E_p=26$ MeV were studied theoretically in the DWA with a microscopic folding model using a realistic nucleon-nucleon interaction and transition densities obtained from Cohen-Kurath p-shell harmonic oscillator wave functions with the size parameter fixed from transverse elastic electron scattering data. A phenomenological optical model was used to generate the distorted waves.

The theoretical calculations provide a reasonable description of the experimental angular distributions. The known Fermi and Gamow-Teller matrix elements for the ground state β decay in mass 11 were used to fix the overall interaction strength from the differential cross section for the ground state (p,n) transition. Estimates of the previously unknown $\langle GT\rangle^2$ matrix elements for the first three excited state transitions in mass 11 were made by normalizing the theoretical differential cross sections obtained with the adjusted interaction to the corresponding experimental cross sections. A simultaneous examination of the available $M1$ electromagnetic matrix elements and the deduced $\langle GT\rangle^2$ was made to study the partition of the positive parity dipole matrix elements for the first four levels in mass 11 into isovector spin and isoscalar spin plus current contributions. In addition, some speculation on the GT strength to higher lying levels in ^{11}C was made on the basis of the (p,n) spectrum in Fig. 1 and the electron scattering work of Ref. 11.

The essential results are that the Cohen-Kurath wave functions do not accurately describe the relative distribution of GT strength in the first four levels of ^{11}C, overestimate the total GT strength to these states, underestimate the net isovector current and isoscalar spin and current contributions to the electromagnetic matrix elements for the corresponding levels in ^{11}B, and quite likely underestimate the GT strength to levels in ^{11}C above the first four states. Specifically, Cohen-Kurath obtain $\sum\langle GT\rangle^2=3.63$ for the total GT strength in ^{11}B(p,n)^{11}C with $\sum\langle GT\rangle^2=2.96$ for the first four levels and $\sum\langle GT\rangle^2=0.67$ for higher lying excitations. From the present (p,n) data and the discussion at the end of Sec. III B it is estimated that $\sum\langle GT\rangle^2_{exp}=1.72$ for the first four levels in ^{11}C and $\sum\langle GT\rangle^2_{exp}\lesssim 1.13$ for higher lying states corresponding to a total $\sum\langle GT\rangle^2\lesssim 2.85$. The latter is 75% of the model value and is consistent with the estimates of the axial vector quenching for p-shell nuclei discussed in Refs. 1 and 22–24.

Since the present manuscript was submitted for publication a 0° ^{11}B(p,n)^{11}C measurement was made with $E_p=160$ MeV at the Indiana University Cyclotron Facility.[35] The preliminary results from this measurement are $\langle GT\rangle^2_{exp}=0.37$ ($E_x=0.0$ MeV), 0.45 ($E_x=2.0$ MeV), 1.05 ($E_x=4.3+4.8$ MeV), 0.47 ($E_x=8.1+8.4$ MeV), 0.39 ($E_x=12.8$ MeV), and 0.29 ($E_x=15.0$ MeV) corresponding to $\sum\langle GT\rangle^2_{exp}=1.87$, 1.15, and 3.02 for the first four levels, higher excitations, and the total strength in ^{11}C, respectively. The total GT strength observed is 83% of the shell model strength. These results are quite consistent with the findings of the present work.

ACKNOWLEDGMENTS

The authors are greatly indebted to T. N. Taddeucci and his collaborators for the use of their unpublished high energy ^{11}B(p,n)^{11}C data and to D. Kurath for specific information and useful discussions concerning the shell model calculations. This work was performed under the auspices of the U.S. Department of Energy by the Lawrence Livermore National Laboratory under Contract No. W-7405-ENG-48 and supported in part by the National Science Foundation under Grant No. PHY-8122131.

*Present address: Department of Physics, Ohio University, Athens, OH 45701.

[1]*The (p,n) Reaction and the Nucleon-Nucleon Force,* edited by C. D. Goodman *et al.* (Plenum, New York, 1980); *Spin Excitations in Nuclei,* edited by F. Petrovich *et al.* (Plenum, New York, 1984).

[2]C. D. Goodman, C. A. Goulding, M. B. Greenfield, J. Rapaport, D. E. Bainum, C. C. Foster, W. G. Love, and F. Petrovich, Phys. Rev. Lett. **44**, 1755 (1980).

[3]D. E. Bainum, J. Rapaport, C. D. Goodman, D. J. Horen, C. C. Foster, M. B. Greenfield, and C. A. Goulding, Phys. Rev. Lett. **44**, 1751 (1980); D. J. Horen, C. D. Goodman, C. C. Foster, C. A. Goulding, M. B. Greenfield, J. Rapaport, D. E. Bainum, E. Sugarbaker, T. G. Masterson, F. Petrovich, and W. G. Love, Phys. Lett. **95B**, 27 (1980).

[4]F. Petrovich and W. G. Love, Nucl. Phys. **A354**, 499c (1981).

[5]W. G. Love and M. A. Franey, Phys. Rev. C **24**, 1973 (1981).

[6]T. N. Taddeucci, J. Rapaport, D. E. Bainum, C. D. Goodman, C. C. Foster, C. Gaarde, J. Larsen, C. A. Goulding, D. J. Horen, T. G. Masterson, and E. Sugarbaker, Phys. Rev. C **25**,

1094 (1982).
[7]G. E. Brown, J. Speth, and J. Wambach, Phys. Rev. Lett. **46**, 1057 (1981).
[8]F. Ajzenberg-Selove and C. L. Busch, Nucl. Phys. **A336**, 1 (1980).
[9]T. Stovall, J. Goldemberg, and D. B. Isabelle, Nucl. Phys. **86**, 225 (1966).
[10]R. E. Rand, R. Frosch, and M. R. Yearian, Phys. Rev. **144**, 859 (1966).
[11]P. T. Kan, G. A. Peterson, D. V. Webb, S. P. Fivozinsky, J. W. Lightbody, Jr., and S. Penner, Phys. Rev. C **11**, 323 (1975).
[12]M. P. Fewell, R. H. Spear, T. H. Zabel, and A. M. Baxter, Aust. J. Phys. **33**, 505 (1980).
[13]R. H. Howell, F. S. Dietrich, D. W. Heikkinen, and F. Petrovich, Phys. Rev. C **21**, 1153 (1980).
[14]R. H. Howell, F. S. Dietrich, and F. Petrovich, Phys. Rev. C **21**, 1158 (1980).
[15]F. Petrovich, R. H. Howell, C. H. Poppe, S. M. Austin, and G. M. Crawley, Nucl. Phys. **A383**, 355 (1982).
[16]S. Cohen and D. Kurath, Nucl. Phys. **73**, 1 (1965); **A101**, 1 (1967).
[17]The spectroscopic coefficients for the wave functions of Ref. 16 are tabulated in T. S. H. Lee and D. Kurath, Phys. Rev. C **21**, 293 (1980).
[18]G. Bertsch, J. Borysowicz, H. McManus, and W. G. Love, Nucl. Phys. **A284**, 399 (1977).
[19]F. Petrovich, W. G. Love, and R. J. McCarthy, Phys. Rev. C **21**, 1718 (1980).
[20]J. Dubach, J. H. Koch, and T. W. Donnelly, Nucl. Phys. **A271**, 279 (1976).
[21]T. Suzuki, S. Krewald, and J. Speth, Phys. Lett. **107B**, 9 (1981).
[22]I. S. Towner and F. C. Khanna, Nucl. Phys. **A399**, 334 (1983).
[23]B. Buck and S. M. Perez, Phys. Rev. Lett. **50**, 1975 (1983).
[24]B. A. Brown and B. H. Wildenthal, Phys. Rev. C **28**, 2397 (1983).
[25]J. C. Davis, J. D. Anderson, E. K. Freytag, and D. R. Rawles, IEEE Trans. Nucl. Sci. **20**, 213 (1973).
[26]B. D. Walker, J. D. Anderson, J. W. McClure, and C. Wong, Nucl. Instrum. Methods **29**, 333 (1964). For the present measurements additional flight paths were constructed. The 30° flight path in the above reference corresponds to 39° in the present measurements since the cyclograff beam line differs from the old Livermore 90-inch cyclotron beam line.
[27]C. Wong, J. D. Anderson, J. C. Davis, and S. M. Grimes, Phys. Rev. C **7**, 1895 (1973).
[28]J. D. Anderson, in *Nuclear Spectroscopy and Reactions*, Part B, edited by J. Cerny (Academic, New York, 1974).
[29]J. D. Anderson, C. Wong, and V. A. Madsen, Phys. Rev. Lett. **24**, 1074 (1970).
[30]K. Ikeda, S. Fujii, and J. I. Fujita, Phys. Lett. **3**, 271 (1961); K. Ikeda, Prog. Theor. Phys. **31**, 434 (1964).
[31]J. J. Kolata and A. Galonsky, Phys. Rev. **182**, 1073 (1969).
[32]R. Schaeffer and J. Raynal, computer code DWBA 70 (unpublished).
[33]L. J. Tassie and F. C. Barker, Phys. Rev. **111**, 940 (1958).
[34]J. R. Comfort, G. L. Moake, C. C. Foster, P. Schwandt, and W. G. Love, Phys. Rev. C **26**, 1800 (1982).
[35]T. N. Taddeucci (private communication).